Konrad-Zuse-Zentrum
für Informationstechnik Berlin

Takustraße 7
D-14195 Berlin-Dahlem
Germany

MARCUS WEBER, ROLAND BECKER, ROBERT KÖPPEN,
VEDAT DURMAZ

Classical hybrid Monte-Carlo simulations of the interconversion of hexabromocyclododecane

ZIB-Report 07-31 (November 2007)

Classical hybrid Monte-Carlo simulations of the interconversion of hexabromocyclododecane*

Marcus Weber, Roland Becker, Robert Köppen, Vedat Durmaz†

November 7, 2007

Abstract

In this paper, we investigate the interconversion processes of the major flame retardant – 1,2,5,6,9,10-hexabromocyclododecane (HBCD) – by the means of statistical thermodynamics based on classical force-fields. Three ideas will be presented. First, the application of classical hybrid Monte-Carlo simulations for quantum mechanical processes will be justified. Second, the problem of insufficient convergence properties of hybrid Monte-Carlo methods for the generation of low temperature canonical ensembles will be solved by an interpolation approach. Furthermore, it will be shown how free energy differences can be used for a rate matrix computation. The results of our numerical simulations will be compared to experimental results.

AMS MSC 2000: 80A17, 82-08

Keywords: Markov process, molecular dynamics, rate matrix.

*Supported by Federal Institute for Materials Research and Testing (BAM), Berlin, Germany.

†Email: weber@zib.de, durmaz@zib.de; address: Zuse-Institute Berlin (ZIB), Takustraße 7, 14195 Berlin. Email: roland.becker@bam.de, robert.koeppen@bam.de; address: Federal Institute for Materials Research and Testing (BAM), Department of Analytical Chemistry, Reference Materials, Richard-Willstätter-Straße 11, 12489 Berlin.

Contents

Introduction

Molecular dynamics simulations based on classical force fields can be used to determine the rate of conformational changes inside the conformational space Ω of small molecules. However, the classical description of molecular motion fails if molecules also partially change their chirality. This is a quantum mechanical process. The timescale of such an *interconversion process* is often far away from the step length of quantum mechanical simulations. In this paper, a simple example for such a situation is presented. The corresponding molecule, 1,2,5,6,9,10-hexabromocyclododecane (HBCD), is shown in Figure 1. We will mainly present three ideas in this paper:

1. It will be explained in Section 1, how classical simulation methods can be used to investigate the interconversion processes of HBCD.

2. It will be shown in Section 4, how the *trapping problem* of low-temperature molecular simulations can be solved by a reweighting approach.

3. In Section 5 it is presented, how free-energy differences and a steady state approximation can be used for a rate matrix computation.

Our goal was to find a classical approach for the estimation of interconversion rates making simulation as simple as possible and, therefore, reproducible. The presented ideas may be the basis for further developments in this field. Our motivation for the use of thermodynamical methods for the investigation of HBCD was the poor prediction results based on single-point quantum chemical calculations. For these calculations, i.e. dipole momentum, polarizability, HOMO and LUMO, we used global minimal potential energy conformations from converging high-temperature simulations (as described below) of the minus enantiomers of each of the three diastereomers in Figure 1. α- and γ-HBCD have the property of c2 symmetry which is missing for β-HBCD. By hint of this property we calculated optimal geometries for each diastereomer, using Gaussian03 with a Becke3LYP/6-31+G* set of basis functions. Unfortunately, there exists no correlation between the predicted water solubility (based on dipol momenta and polarizability and confirmed by similar results of other publications [1, 32]) with experimental results [22]. This observation leads us to the assumption that it is hardly possible to generalize the output from a single-point calculation based on one conformation to a whole ensemble of conformations, as it usually occurs in reality. It is necessary to consider a molecular system as an ensemble of many different states, each holding (slightly) different molecular properties. In this article, transition rates are not estimated using saddle-point energy computations, but they are derived from classical thermodynamics simulations.

1 The isomerism of HBCD and the interconversion mechanism

HBCD is one of the major flame retardant additives to plastics and it is increasingly found in trace amounts in the environment, biota, and humans [6, 7, 8, 28]. Therefore, HBCD is currently one of the emerging environmental analytes of interest. There is evidence for activity of HBCD as endocrine disruptor [33] and

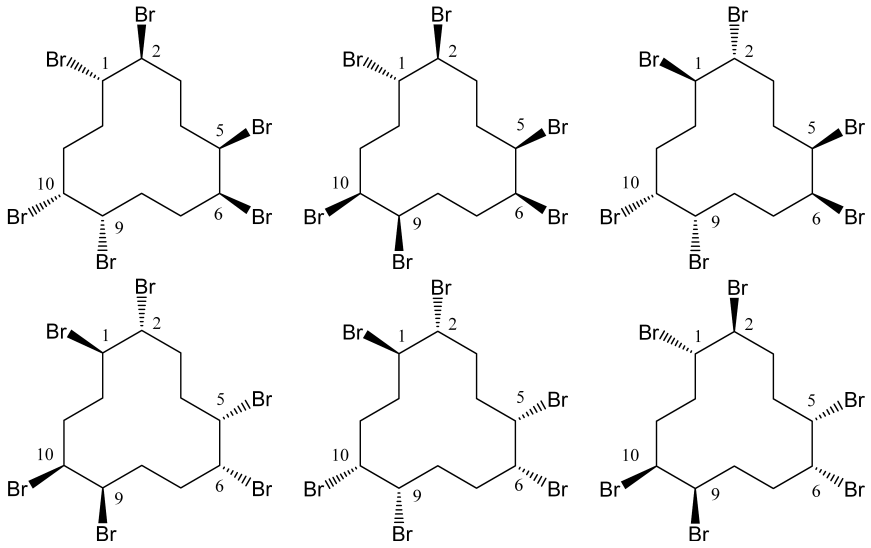

Figure 1: Different stereoisomers of technical HBCD. *Top row from left to right:* (+)-α-HBCD, (+)-β-HBCD, (+)-γ-HBCD. *Bottom row from left to right:* (−)-α-HBCD, (−)-β-HBCD, (−)-γ-HBCD.

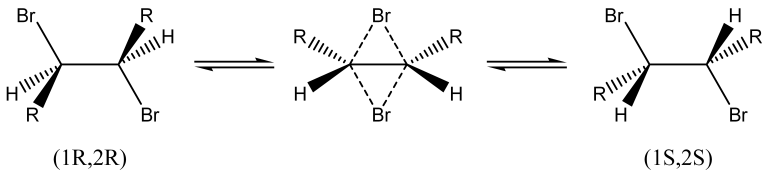

Figure 2: Interconversion mechanism for HBCD. The interconversion is only possible if the two bromine atoms are in anti-position.

an EU risk assessment is under way. Technical HBCD consists mainly of three diastereomeric pairs of enantiomers (Figure 1). The absolute configurations of enantiomers were only recently correlated with their order of chromatographic elution [27]. In the absence of a chiral environment, the (−)-enantiomers behave in the same way as the (+)-enantiomers. Therefore, in the followings we only investigate the (+)-enantiomers. The results for the (−)-enantiomers (e.g., in Tables 5-7) can be derived by simply changing sign. We are interested in the interconversion of the HBCD stereoisomers shown in Figure 1 because it is important to understand their behavior in technical processes and gas chromatographic analysis. Furthermore, the diastereomeric and enantiomeric composition in biological samples differ from that of technical mixture and the biological induced interconversion of HBCD at ambient temperature is discussed [28]. The chemical mechanism of the transition between these structures is shown in Figure 2: Two vicinal bromine atoms change their positions with two hydrogen atoms under inversion of absolute configurations. This is a quantum mechanical process. The interconversion can only take place, if the bromine

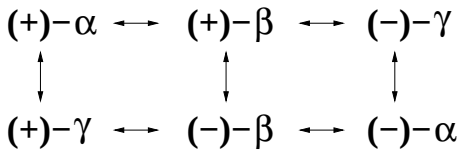

Figure 3: Possible interconversion reactions of the HBCD isomers connected to the three sets of vicinal bromine atoms.

atoms are in anti-position. Once the bromine atoms are in anti-position, the rate of the interconversion process can be seen as largely independent from the structure of the rests R in Figure 2. Such a reaction has been denoted as cyclic-concerted mechanism and was so far only investigated on variously substituted 1,2-dibromocyclohexane systems [2, 3, 4, 16, 25]. In case of HBCD there are three sets of vicinal bromine atoms each being able to undergo the concerted interconversion and at the same time mutually influencing the conformational alignment of the cyclododecane ring and resulting in diastereomer-specific distribution of conformers. It was shown experimentally [23, 29, 19] that a mixture containing α-, β-, and γ-HBCD in any composition interconverts towards an equilibrium which is dominated by α-HBCD. The reaction pathways are depicted in Figure 3. This leads to the following idea, that classical simulation can be used in order to characterize the interconversion processes qualitatively. Via computer simulation and for every dihedral angle (C1C2, C5C6, C9C10) in Figure 1, we will determine the part of the configurational space of (+)-α-HBCD, (+)-β-HBCD, and (+)-γ-HBCD for which the dihedral angle is in anti-position compared to the part of the configurational space, where the angle is in gauche-position. These results are presented in terms of free energy differences in Tables 5-7. The more the anti-position is preferred, the faster the conversion at the corresponding dihedral angle will occur. The basis for our simulations will be the *Boltzmann* distribution (canonical ensemble) of states. This is the most likely distribution of states at constant temperature, constant number of particles and constant volume. Since the interconversion of neat HBCD only takes place above its melting point at about 430 K, this will be the temperature of interest. As an approximation, the simulations in this paper are performed for the vacuum.

2 Experimental results

The experimental set-up is discussed in detail elsewhere [26]. In brief, pure (+)-γ-HBCD is exposed to 160°C for different periods between two and 60 minutes and then the concentrations of all six stereoisomers (Figure 1) are determined for each point in time by liquid chromatography with diode array detection using a chiral column. Since no other compound including different HBCD isomers were detected, the sum concentration of the six HBCD stereoisomers measured at a particular time was set to 100% for each point in time. Then, the molar fraction of each diastereomer was calculated as mol-(%). The Mathematica 4.0 software package from Wolfram Research, Inc. (USA) was used for a parameter estimation of the kinetic constants. For this purpose, the time dependet

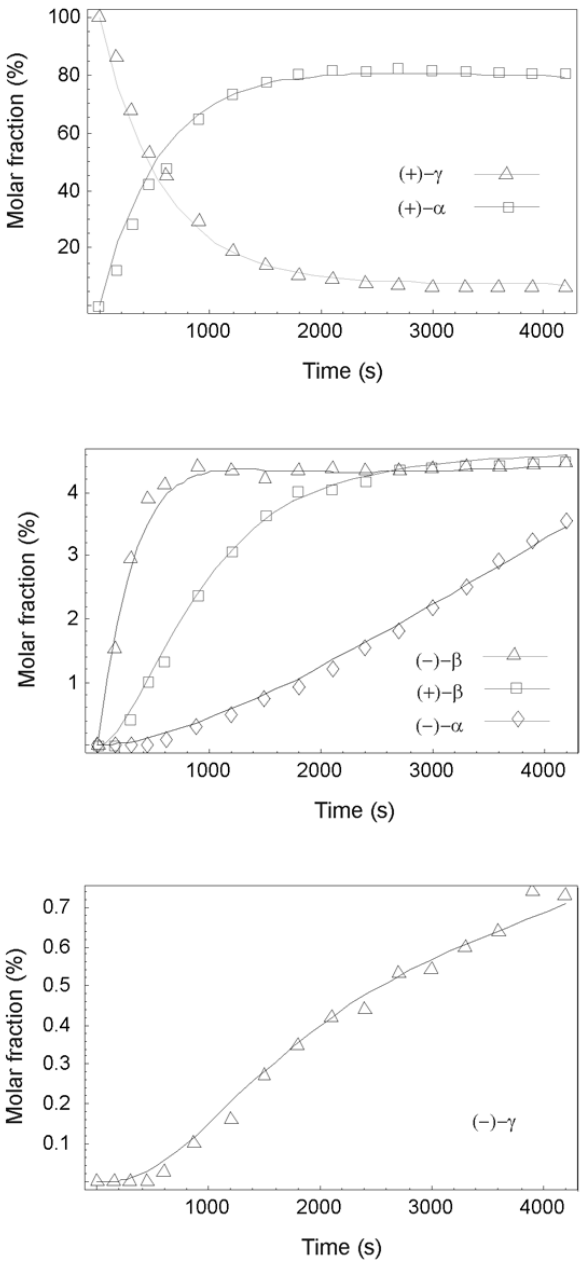

Figure 4: Interconversion experiment starting with 100% (+)-γ-HBCD.

concentration vector $x \in \mathbb{R}^6$ is modelled as a solution of a rate equation

$$\frac{d\,x(t)}{dt} = Q^\top\, x(t), \tag{1}$$

where $Q \in \mathbb{R}^{6\times 6}$ is the corresponding rate matrix and x is the vector of the concentrations of the six species of Figure 1 (in the corresponding order: (+)-α, (+)-β, (+)-γ, (−)-α, (−)-β, (−)-γ). The least squares fit of the experimental data correspods to the following rate matrix result

$$Q^{exp.} = 0.001\cdot \begin{pmatrix} -0.1608 & 0.0188 & 0.1420 & 0 & 0 & 0 \\ 0.1200 & -1.3900 & 0 & 0 & 1.1000 & 0.1700 \\ 1.5000 & 0 & -1.6460 & 0 & 0.1460 & 0 \\ 0 & 0 & 0 & -0.1608 & 0.0188 & 0.1420 \\ 0 & 1.1000 & 0.1700 & 0.1200 & -1.3900 & 0 \\ 0 & 0.1460 & 0 & 1.5000 & 0 & -1.6460 \end{pmatrix}.$$

The corresponding time-dependend concentration plots are shown in Figure 4.

3 Hybrid Monte-Carlo simulation

In the *Boltzmann* distribution of states at temperature T, the probability $\pi(q)$ for a conformation $q \in \Omega$ of the conformational space Ω is proportional to

$$\pi(q) \propto \exp(-\beta\, V_{pot}(q)) \tag{2}$$

with the inverse temperature

$$\beta = 1/(T * 0.008314403 \frac{kJ}{mol\cdot K}) \Rightarrow \beta \propto 1/T. \tag{3}$$

In (2), $V_{pot} : \Omega \to \mathbb{R}$ is the potential energy of the conformational states. For our classical simulations, this function is given by the Merck Molecular Force Field which has been designed for small molecules like HBCD [17, 18]. In order to generate a set of states (a trajectory of states) distributed according to (2), we applied the hybrid Monte-Carlo method (HMC) [9, 30]. This method is a combination of a Markov Chain Monte-Carlo approach with short time (78 fs using a velocity verlet integrator [12] with a time-step of 1.3 fs) molecular dynamics (MD) simulations. The initial momenta for the MD part of the algorithm are taken from the Boltzmann-distribution of momenta at the given temperature. Unfortunately, the HMC-method rarely overcomes high potential energy barriers [10, 11]. Only if the kinetic energy of the initial momenta is high enough, the HMC-method is able to reach the important parts of the conformational space. For this reason, we have simulated the three molecules at an artificial high temperature $T = 1500\,K$ with $\beta_0 = 0.08018\,mol/kJ$. In a first computer experiment, we compared the results of five different HMC-samplings, each of them consisting of $10,000$ steps. The proposed Gelman-Rubin convergence indicator (convergence value = 1.1; observables = sine and cosine of dihedral angles) was not reached after this number of sampling steps [13, 14]. In addition, the symmetry of the γ-structure was not reflected by the sampling data. Therefore, we performed a HMC-sampling with $100,000$ steps. In this case, the convergence indicator was reached and the symmetry of the

$\alpha-$ and the $\gamma-$structure could also be found in the sampling data. We also performed samplings with $5 \times 100,000$ steps for each of the $(-)$-structures and found the same symmetries and results. The bad convergence properties lead us to an academic question: Due to the low convergence rate, we can conclude that there are dynamical metastabilities inside the ring structure. This may be a reason for non-existence of stereoisomer-specific interconversion rates. In order to write down interconversion rates from, e.g., (+)-α-HBCD to another stereoisomer of HBCD, we have to assume, that each isomer can be seen as one kinetic species. But each metastable subset of the conformational space of, e.g., (+)-α-HBCD may have a different dynamical behavior (and may, therefore, be an own species from the kinetic point of view). Only, if the timescale of conformational changes within the conformational space of the HBCD isomers is much shorter than the timescale of interconversion, the postulation of interconversion rates makes sense. From experiments we can conclude that the timescale of interconversion is in the range of seconds. This is the timescale of protein folding. HBCD is much smaller and more flexible than a protein. This means, that the definition of interconversion rates is reasonable. We are interested in the thermodynamics of the molecules at low temperature $T = 430\,K$ with $\beta_1 = 0.27971\,mol/kJ$. Thus, in a first step, we derive thermodynamical values from the HMC sampling for $T = 1500\,K$. In a second step, we reweight these quantities to low temperature. One thermodynamic value is the free energy A of the system. It is given by the partition function

$$A(\beta) = -\frac{1}{\beta} \ln \Big(\int_{\Omega} \exp(-\beta\, V_{pot}(q))\, dq \Big). \tag{4}$$

In equation (4), the kinetic energy part of A is missing. This simplification is possible, because we are only interested in free energy differences. Furthermore, potential and kinetic energy are separable and the kinetic energy part is identical for the observed subsystems. The integral in (4) can not be approximated by numerical methods. But ratios of integrals over certain subsets of Ω can be approximated, i.e. free energy differences can be computed. For a given dihedral angle θ, we are interested in the portion of states that can be seen as *anti* compared to the portion of states that are *gauche* with respect to θ. In the present application, we defined dihedral angles $120^\circ \geq \theta \geq -120^\circ$ as *gauche*. With this separation of states, we have determined free energy differences from the HMC-sampling by counting the different states N_{anti} and N_{gauche} respectively and applying

$$\Delta_{ga} A(\beta) \approx -\frac{1}{\beta} \ln \Big(\frac{N_{gauche}}{N_{anti}} \Big). \tag{5}$$

The results are given in Tables 1-3. The more negative $\Delta_{ga}A$ the more the *gauche* states are preferred. Another interesting value can be derived from the

(+)-α-HBCD		$\langle V_{pot} \rangle = 921$
C1C2	$\Delta_{ga}A$ = -17	$\Delta_{ga}\langle V_{pot} \rangle$ = -8
C5C6	$\Delta_{ga}A$ = -40	$\Delta_{ga}\langle V_{pot} \rangle$ = -26
C9C10	$\Delta_{ga}A$ = -40	$\Delta_{ga}\langle V_{pot} \rangle$ = -25

Table 1: Free energy differences $\Delta_{ga}A$, mean potential energy $\langle V_{pot} \rangle$ and mean potential energy differences $\Delta_{ga}\langle V_{pot} \rangle$ of (+)-α-HBCD at T=1500 K in kJ/mol.

(+)-β-HBCD		$\langle V_{pot} \rangle = 931$
C1C2	$\Delta_{ga} A$ = -14	$\Delta_{ga} \langle V_{pot} \rangle = 0$
C5C6	$\Delta_{ga} A$ = -36	$\Delta_{ga} \langle V_{pot} \rangle$ = -20
C9C10	$\Delta_{ga} A$ = -34	$\Delta_{ga} \langle V_{pot} \rangle$ = -17

Table 2: Free energy differences $\Delta_{ga} A$, mean potential energy $\langle V_{pot} \rangle$ and mean potential energy differences $\Delta_{ga} \langle V_{pot} \rangle$ of (+)-β-HBCD at T=1500 K in [kJ/mol].

(+)-γ-HBCD		$\langle V_{pot} \rangle = 926$
C1C2	$\Delta_{ga} A$ = -10	$\Delta_{ga} \langle V_{pot} \rangle = 5$
C5C6	$\Delta_{ga} A$ = -41	$\Delta_{ga} \langle V_{pot} \rangle$ = -28
C9C10	$\Delta_{ga} A$ = -41	$\Delta_{ga} \langle V_{pot} \rangle$ = -27

Table 3: Free energy differences $\Delta_{ga} A$, mean potential energy $\langle V_{pot} \rangle$ and mean potential energy differences $\Delta_{ga} \langle V_{pot} \rangle$ of (+)-γ-HBCD at T=1500 K in [kJ/mol].

simulations: The mean potential energy value

$$\langle V_{pot} \rangle(\beta) = \int_{\Omega} V_{pot}(q) \frac{\exp(-\beta\, V_{pot}(q))}{\int_{\Omega} \exp(-\beta\, V_{pot}(q))\, dq}\, dq. \tag{6}$$

The inner energy $\langle V_{tot} \rangle$ of the system is the sum

$$\langle V_{tot} \rangle = \langle V_{pot} \rangle + \langle V_{kin} \rangle \tag{7}$$

of the mean potential and the mean kinetic energy. Numerically, $\langle V_{pot} \rangle$ can be approximated by the mean of the potential energy values of the HMC-sampling. Mean potential energy differences can also be computed if we split the set of states into anti- and gauche-conformations. The corresponding results are also presented in the Tables 1-3.

4 Reweighting formula

In a second step, we have to reweight the sampling data from the high-temperture sampling with $T = 1500\,K$ to $T = 430\,K$. The term "reweighting" is mostly used for the following method: A statistical weight is assigned to every generated data-point from the high-temperature sampling. One tries to adjust these weights in order to approximate the low-temperature distribution of energies. This procedure often fails: In a high temperature sampling the potential energy values are distributed in a broader range with a higher mean value compared to a low-temperature sampling, see Figure 5. Most of the sampling points have a high potential energy value. If we aim at a reweighting of the sampling points in order to get the low-temperature distribution, the low-energy points of the high-temperature sampling are weighted up statistically. Therefore, point-wise reweighting schemes only make use of the sampling points located in the small overlap region of the high-temperature and the low-temperature distribution. The occupation of this region depends on the input parameters of the algorithms very sensitively. The common opinion is that reweighting is only possible for sufficiently overlapping distributions. This opinion led to many sophisticated (but not simple) sampling methods in the past. The most famous one is replica

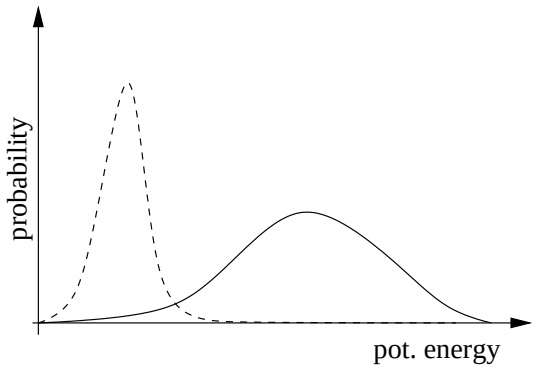

Figure 5: The distribution of the potential energy values for different temperatures. *Solid line:* High temperature. *Dashed line:* Low temperature.

exchange [31]. Other examples can be found in modern textbooks [5]. In our case, we will see that it is not important to approximate the complete distribution of states at the lower temperature. It is sufficient to know, how the mean value in Figure 5 depends on the temperature. Instead of a point-wise reweighting scheme, we present a thermodynamical approach in this work. For the purpose of simplicity we set $U := \langle V_{pot} \rangle$ for the mean potential energy in the followings. As an approximation, we assume that the mean potential energy U depends linearily on the temperature T of the system. In this case $\Delta U(\beta)$ goes with $1/\beta$ due to (3), i.e

$$\Delta U(\beta) = \frac{(\Delta U(\beta_0) - \Delta U(\infty))\,\beta_0}{\beta} + \Delta U(\infty). \tag{8}$$

Since the mean kinetic energy $\langle V_{kin} \rangle$ in (7) depends linearly on the temperature, the assumption (8) is equivalent to a linear model for the inner energy $\langle V_{tot} \rangle$ of the system. Furthermore, assuming a linear model for the inner energy in reality would mean that the heat capacity C_V is a temperature-independend constant. This assumption is not true, but mostly according to quantum effects which are not part of the classical model used in this work. From the classical viewpoint, (8) is exact, if the potential energy V_{pot} is a quadratic function. It is a good approximation, if the conformation space Ω can be decomposed, such that each part of this decomposition has a *Gaussian*-like *Boltzmann* distribution. This is a widely used assumption in many applications. More details can be found in Appendix A. In order to apply (8), we have to compute the limit $\Delta U(\infty)$. With increasing β, the Boltzmann-distribution more and more focusses on the global optimum of the system. In our case, we have split our system into two parts: the anti- and the gauche-states. The limit of ΔU for increasing β is equivalent to the difference $\Delta_{ga} V^0_{pot}$ of the lowest potential energy values of the two subsystems, i.e. $\Delta_{ga} V^0_{pot} = \Delta U(\infty)$. The entries in Table 4 are the results of local minimizations (using the *conjugate gradient* method [21]) applied to each point of the trajectories of the given high-temperature HMC-samplings. The gauche-position of the bromine atoms is always preferred. This also corresponds to the experiment: All known crystal structures of HBCD stereoisomers display all-gauche configuration of all vicinal bromine atoms [27, 19, 20]. The mean

(+)-α-HBCD	gauche	anti	$\Delta_{ga}V^0_{pot}$
C1C2	239	253	-14
C5C6	239	272	-33
C9C10	239	272	-33
(+)-β-HBCD	gauche	anti	$\Delta_{ga}V^0_{pot}$
C1C2	249	264	-15
C5C6	249	285	-36
C9C10	249	276	-27
(+)-γ-HBCD	gauche	anti	$\Delta_{ga}V^0_{pot}$
C1C2	257	257	0
C5C6	257	275	-18
C9C10	257	275	-18

Table 4: Lowest potential energy value V^0_{pot} for the anti and gauche conformations and their differences $\Delta_{ga}V^0_{pot}$ in kJ/mol.

potential energy values $\langle V_{pot}\rangle$ according to a linear model (8) are presented in the Tables 5-7. In order to interpret reaction rates, we are not interested in the mean potential energy values but in free energy differences $\Delta_{ga}A(\beta)$. The β-dependency of A can be calculated by differentiating (4) and inserting (6):

$$\frac{d}{d\beta}\Delta_{ga}A(\beta) = -\frac{1}{\beta}\Delta_{ga}A(\beta) + \frac{1}{\beta}\Delta_{ga}\langle V_{pot}\rangle(\beta). \tag{9}$$

Using the linear model (8) for U provides

$$\frac{d}{d\beta}\Delta_{ga}A(\beta) = -\frac{1}{\beta}\Delta_{ga}A(\beta) + \frac{(\Delta U(\beta_0) - \Delta U(\infty))\,\beta_0}{\beta^2} + \frac{\Delta U(\infty)}{\beta}. \tag{10}$$

The orinary differential equation (10) can be solved analytically, such that

$$\Delta_{ga}A(\beta) = \frac{1}{\beta}\big((\beta-\beta_0)\,\Delta U(\infty) + \ln\Big(\frac{\beta}{\beta_0}\Big)\,\beta_0\,(\Delta U(\beta_0) - \Delta U(\infty)) + \beta_0\,\Delta_{ga}A(\beta_0)\big) \tag{11}$$

for an initial value $\Delta_{ga}A(\beta_0)$ which can be found in Tables 1-3. Via formula (11) and the corresponding values for $\Delta U(\beta_0)$, $\Delta U(\infty)$, and $\Delta_{ga}A(\beta_0)$ the free energy differences can be computed for $430\,K$. The results are given in the Tables 5-7. In contrast to a point-wise reweighting scheme, formula (11) is robust against small perturbations of the input data.

5 Rate matrix computation

In Tables 5-7, the results of the reweighting formula are presented. The most important questions are: How do these simulation results fit to the experimental results? Do they reflect the qualitative behavior of the HBCD-system? In order to answer these questions, the meaning of the simulation results for the qualitative behavior of the HBCD-system will be visualized in the followings. From a mathematical point of view, we will apply the *Arrhenius* equation [15]:

$$k \propto \exp(-\beta\,\Delta_{ag}A). \tag{12}$$

(+)-α-HBCD	$\langle V_{pot}\rangle$ = 435 kJ/mol	interconv. to ...
C1C2	$\Delta_{ga}A$ = -13 kJ/mol	(+)-γ-HBCD
C5C6	$\Delta_{ga}A$ = -33 kJ/mol	(+)-β-HBCD
C9C10	$\Delta_{ga}A$ = -32 kJ/mol	(+)-β-HBCD

Table 5: Free energy differences $\Delta_{ga}A$ and mean potential energy $\langle V_{pot}\rangle$ of (+)-α-HBCD at T=430 K.

(+)-β-HBCD	$\langle V_{pot}\rangle$ = 445 kJ/mol	interconv. to ...
C1C2	$\Delta_{ga}A$ = -9 kJ/mol	(−)-β-HBCD
C5C6	$\Delta_{ga}A$ = -30 kJ/mol	(−)-γ-HBCD
C9C10	$\Delta_{ga}A$ = -25 kJ/mol	(+)-α-HBCD

Table 6: Free energy differences $\Delta_{ga}A$ and mean potential energy $\langle V_{pot}\rangle$ of (+)-β-HBCD at T=430 K.

In this approach, the reaction rate k of an interconversion is propotional to the *Boltzmann* expression of the activation energy. With $\Delta_{ag}A = -\Delta_{ga}A$, the free energy differences in Tabels 5-7 can be used to estimate these activation energies. On the basis of these considerations, a rate matrix $Q \in \mathbb{R}^{6\times 6}$ will be constructed for the six species of Figure 1 (in the corresponding order: (+)-α, (+)-β, (+)-γ, (−)-α, (−)-β, (−)-γ). The model is based on the rate equation (1) with the concentration vector $x \in \mathbb{R}^6$. It is known from theory [24], that the rate matrix Q of this *Markov* process can be written in the form

$$Q = R\,(K - id), \tag{13}$$

where id is the six-dimensional unit matrix, $K \in \mathbb{R}^{6\times 6}$ is the *embedded Markov chain* and $R \in \mathbb{R}^{6\times 6}$ is a diagonal matrix of *rate factors*. On the basis of the free energy differences and (12), the *embedded Markov chain* can be computed by inserting the values of the Arrhenius equation into a matrix and rescaling the rows, such that the row sums are 1. For HBCD, it has to be taken into account that there are sometimes two different ways for an interconverion from one stereoisomer to another (muliplication of k with factor 2):

$$K = \begin{pmatrix} 0 & 0.0074 & 0.9926 & 0 & 0 & 0 \\ 0.0112 & 0 & 0 & 0 & 0.9860 & 0.0028 \\ 0.9990 & 0 & 0 & 0 & 0.0010 & 0 \\ 0 & 0 & 0 & 0 & 0.0074 & 0.9926 \\ 0 & 0.9860 & 0.0028 & 0.0112 & 0 & 0 \\ 0 & 0.0010 & 0 & 0.9990 & 0 & 0 \end{pmatrix}.$$

For the computation of the rate factors, it can be used that the equilibrium concentration of the six species is a steady state of equation (1). We will not use experimental data in order to determine the steady state vector $\pi \in \mathbb{R}^6$. The equilibrium concentrations can be estimated by the mean potential energy values in Tables 5-7 and the *Boltzmann* expression (2) instead (replace V_{pot} by $\langle V_{pot}\rangle$). The result is

$$\pi^\top = (0.4626,\ 0.0282,\ 0.0092,\ 0.4626,\ 0.0282,\ 0.0092).$$

(+)-γ-HBCD	$\langle V_{pot} \rangle$ = 449 kJ/mol	interconv. to ...
C1C2	$\Delta_{ga}A$ = -1 kJ/mol	(+)-α-HBCD
C5C6	$\Delta_{ga}A$ = -28 kJ/mol	(−)-β-HBCD
C9C10	$\Delta_{ga}A$ = -28 kJ/mol	(−)-β-HBCD

Table 7: Free energy differences $\Delta_{ga}A$ and mean potential energy $\langle V_{pot} \rangle$ of (+)-γ-HBCD at T=430 K.

Up to an unknown scaling factor $\mu > 0$, there is a unique solution for R, for which π is the steady state of Q on the basis of K and (13). This solution $r \in \mathbb{R}^6$ is given by the linear equation

$$r^\top D(K - id) = 0, \tag{14}$$

where K is given by the *Arrhenius* approximation, D is the diagonal matrix $D = \mathrm{diag}(\pi)$ of the given steady state solution, and r is the unkown vector of rate factors, with $R = \mathrm{diag}(r)$. In our case, this means

$$Q^{theo.} = \mu \cdot \begin{pmatrix} -0.0200 & 0.0001 & 0.0199 & 0 & 0 & 0 \\ 0.0022 & -0.1978 & 0 & 0 & 0.1950 & 0.0005 \\ 0.9990 & 0 & -1.0000 & 0 & 0.0010 & 0 \\ 0 & 0 & 0 & -0.0200 & 0.0001 & 0.0199 \\ 0 & 0.1950 & 0.0005 & 0.0022 & -0.1978 & 0 \\ 0 & 0.0010 & 0 & 0.9990 & 0 & -1.0000 \end{pmatrix}.$$

For more details about the determination of Q, see also [35]. For this matrix Q, a kinetic simulation of (1) is shown in Figure 6. $\mu = 0.001$ has been fixed "by eye". μ is not available via classical methods because of the unknown interconversion rate (see Figure 2). The kinetic simulation has been performed for the initial condition of the kinetic experiment (Figure 4). Although there have been so many sources of error (classical approach, vacuum, *Boltzmann* distribution, reweighting to $430K$, *Arrhenius* equation, ..., see Appendix B), the correct qualitative behavior of the system can be seen in the plots: The different increase of the (+)-β-HBCD and the (−)-β-HBCD concentration. The initial increase of the (+)-α-HBCD concentration far above its equillibrium value. The low initial concentrations of (−)-α-HBCD and (−)-γ-HBCD. Thus, we can conclude that the numerical simulations reflect qualitatively the behavior of the HBCD-system. A detailed comparison of K and $Q^{theo.}$ with the experimental results ($Q^{exp.}$ on page 7) provides the following analogies:

1. α-HBCD converts faster into γ-HBCD (and much slower into β-HBCD),
2. (+)-β-HBCD converts faster into (−)-β-HBCD, and vice versa,
3. γ-HBCD converts faster into α-HBCD,
4. the dominating reaction is the interconversion from γ-HBCD to α-HBCD.

Conclusion

We have investigated the interconversion processes of HBCD. These are quantum mechanical processes which take place on a timescale of seconds. Due to

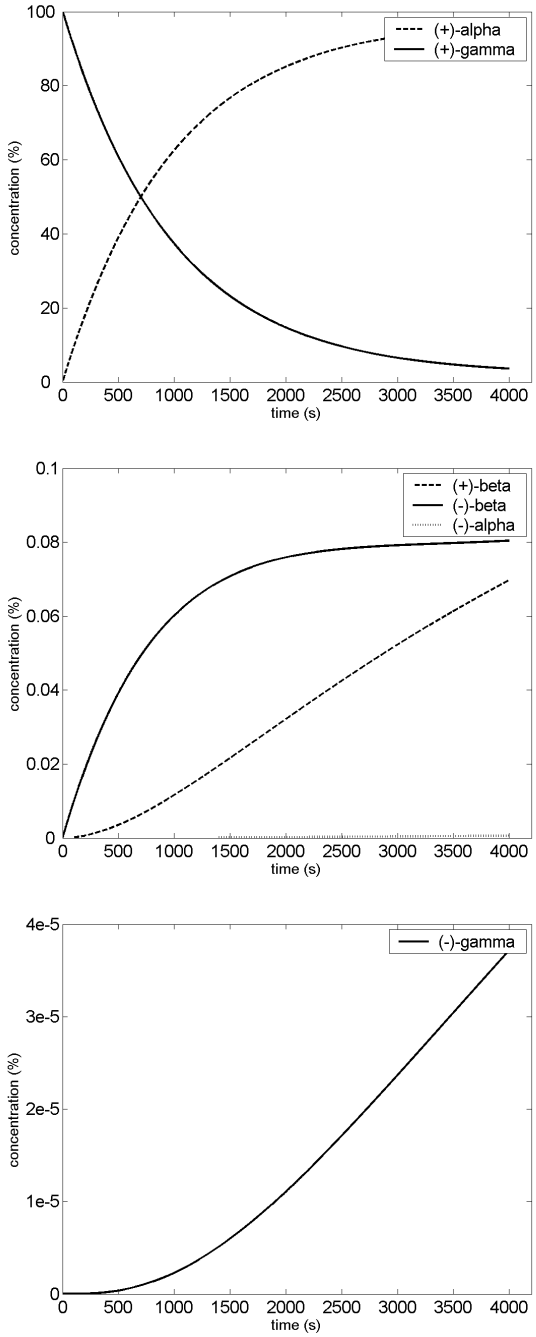

Figure 6: Qualitative behavior of interconverion based on free energy computations

very different timescales, quantum mechanical molecular simulation algorithms are not applicable for an analysis of these processes. But, whenever the quantum mechanical mechanism is identical for all interconversion processes, it is only important to know which part of the conformational space initializes the process. Then, based on classical simulations, one can compute the portion of the conformational space which can be seen as *activated*. This portion is a measure for the corresponding transition rate. In our example, even the classical simulation algorithm has to tackle very different timescales and only high temperature HMC-samplings are able to provide correct thermodynamical ensembles. We have presented a simple reweighting formula which can be used to interpolate the important thermodynamical values at lower temperature. With all these simplifications, the HMC-samplings for each of the HBCD-stereoisomers needed 30 million force field evaluations (CPU-time on our simple PC: 6 hours).

Outlook. The presented ideas use the fact that the unknown rate of the interconversion mechanism in Figure 2 is identical for each transition in Figure 3. In this case, the time scale factor μ is the only unknown value in the rate matrix computation. If the interconversion mechanism is different for each of the interconversion processes, the above scheme for the rate matrix computation is also valid. In this case, we have to estimate the activation energy of the corresponding interconversion mechanism in Figure 2, e.g., by the means of quantum-based transition state computations. This additional activation energy has to be inserted into the *Arrhenius* equation (12), too. This means a combination of insufficient single-point quantum chemistry calculations with results of classical thermodynamics simulations.

Acknowledgement. This work was supported in the framework of the BAM-ZIB co-operation on common research and developement in the field of scientific computing. Date of agreement: July 10th, 2007.

A Temperature dependence of the mean potential energy

In order to justify the linear model for the mean potential energy in (8), it will be shown that this behavior is valid for quadratic potentials $V_{pot} : \mathbb{R}^d \to \mathbb{R}$. This also justifies the application of a linear model for multivariate *Boltzmann* distributions which are locally *Gaussian* (approximately locally quadratic potential engergy functions). Without loss of generality (and via principle axis transformation), the d-dimensional quadratic potential energy function can be written in separable form:

$$V_{pot}(q) = \sum_{i=1}^{d} (a_i\, q_i^2 + b_i\, q_i + c_i) := \sum_{i=1}^{d} V_i(q_i) \tag{15}$$

with corresponding constants $a_i, b_i, c_i \in \mathbb{R}$ and $a_i > 0$. A short calculation on the basis of (6) and (15) yields

$$\langle V_{pot} \rangle = \sum_{i=1}^{d} \int_{-\infty}^{\infty} V_i(q_i) \frac{\exp(-\beta\, V_i(q_i))}{\int_{-\infty}^{\infty} \exp(-\beta\, V_i(q_i))\, dq_i}\, dq_i. \tag{16}$$

Equation (16) shows that the linear dependency of the mean potential energy can be justified by solving the integral in (6) for the 1-dimensional case. The result is

$$\langle V_{pot}\rangle = \sum_{i=1}^{d} \frac{1}{2\beta} - \frac{b_i^2}{4a_i} + c_i \tag{17}$$

which is exactly the claimed $1/\beta$-behavior of $\langle V_{pot}\rangle$. With $b_i = 0$ and $c_i = 0$, equation (17) is the well-known $1/2\,kT$-contribution per degree of freedom to the inner energy of an ideal gas. For a numerical justification of the linear temperature dependence, we performed two HMC samplings of (+)-α-HBCD at $T = 430\,K$. One sampling started in the low energy region of the optimal conformation of (+)-α-HBCD and one sampling started in an high-energy region. After $5 \times 10,000$ steps the samplings did not converge (as expected). The mean potential energy values were $420\,kJ/mol$ and $455\,kJ/mol$, respectively. They are lower and upper bounds for the true value. From the mean potential energy $\langle V_{pot}\rangle = 921\,kJ/mol$ at high temperature and an optimal value $V_{pot}^0 = 239\,kJ/mol$ of the potential energy, the linear model (8) predicts a mean energy of $435\,kJ/mol$ at a temperatur of $430K$ in accordance with the simulated bounds. For a better verification of the reweighting formula, we performed an extensive simulation with the inhouse software ZIBgridfree [34] and a pointwise density estimation strategy [36]. The simulated mean potential energy $434\,kJ/mol$ is very close to the calculated value $435\,kJ/mol$ of the reweighting formula. For all these reasons, we think that the reweighting formula is applicable.

B Medium temperature results

Quantitatively, the simulation results of Section 5 do not predict the experimental results. In fact, a lot of approximations have been used. The severest one may be the vacuum-approximation. Liquid HBCD has a dielectric constant which is different from the vacuum. Also the interactions between the HBCD molecules in a liquid phase can not be neglected. Briefly, the energy barriers and the energy differences are overestimated by the classical model in Section 5. From a statistical point of view, a simple downscaling of the potential energy function is equivalent to increasing the temperature. And, in fact, for a temperature of $T = 670\,K$, we get the steady state estimation:

$$\pi^\top = (0.3912,\ 0.0650,\ 0.0438,\ 0.3912,\ 0.0650,\ 0.0438),$$

which perfectly fits to experimental results [1, 29] (78% α-HBCD, 14% β-HBCD, and 8% γ-HBCD). Furthermore, for this medium temperature, the main interconversion rates ($\alpha \rightleftharpoons \gamma$ and $\beta \rightleftharpoons \beta$) with $\mu = 0.0015$ also perfectly fit to the experiment:

$$Q^{theo.} = 0.001 \cdot \begin{pmatrix} -0.1730 & 0.0084 & \mathbf{0.1646} & 0 & 0 & 0 \\ 0.0405 & -0.9764 & 0 & 0 & \mathbf{0.9152} & 0.0208 \\ \mathbf{1.4843} & 0 & -1.5000 & 0 & 0.0157 & 0 \\ 0 & 0 & 0 & -0.1730 & 0.0084 & \mathbf{0.1646} \\ 0 & \mathbf{0.9152} & 0.0208 & 0.0405 & -0.9764 & 0 \\ 0 & 0.0157 & 0 & \mathbf{1.4843} & 0 & -1.5000 \end{pmatrix}.$$

References

[1] G. Arsenault, B. Chittim, A. McAlees, and R. McCridle. Nuclear magnetic resonance spectral characterization and semi-empirical calculations of conformations of α- and γ-1,2,5,6,9,10-hexabromocyclododecane. *Chemosphere*, 67:1684–1694, 2007.

[2] P.L. Barili, G. Bellucci, G. Berti, A. Marioni, A. Marsili, and I. Morelli. Thermal equilibrium of substituted trans-1,2-dibromocyclohexanes. *J. Chem. Soc. Perk. T.*, 2(1):58–62, 1972.

[3] F. Barontini, V. Cozzani, and L. Petarca. Thermal stability and decomposition products of hexabromocyclododecane. *Ind. Eng. Chem. Res.*, 40:3270–3280, 2001.

[4] G. Bellucci, A. Marsili, E. Mastrorilli, I. Morelli, and V. Scartoni. Kinetics of thermal racemization of some 1,2-dihalides. *J. Chem. Soc. Perk. T.*, 2(2):201–204, 1972.

[5] Ch. Chipot and A. Pohorille, editors. *Free Energy Calculations*. Number 86 in Springer series in chemical physics. Springer, Berlin, Heidelberg, 2007.

[6] A. Covaci, A.S.C. Gerecke, R.J. Law, S. Voorspoels, M. Kohler, N.V. Heeb, H. Leslie, C.R. Allchin, and J. DeBoer. Hexabromocyclododecanes (hbcds) in the environment and humans: a review. *Environ. Sci. Technol.*, 40:3680–3688, 2006.

[7] C. A. de Wit. An overview of brominated flame retardants in the environment. *Chemosphere*, 40:583–624, 2002.

[8] C. A. de Wit, M. Alaee, and D.C.G. Muir. Levels and trends of brominated flame retardants in the arctic. *Chemosphere*, 64:209–233, 2006.

[9] S. Duane, A. D. Kennedy, B. J. Pendleton, and D. Roweth. Hybrid Monte Carlo. *Phys. Lett. B*, 195(2):216–222, 1987.

[10] A. Fischer. *An Uncoupling–Coupling Method for Markov Chain Monte Carlo Simulations with an Application to Biomolecules*. Doctoral thesis, Freie Universität Berlin, 2003.

[11] A. Fischer, Ch. Schütte, P. Deuflhard, and F. Cordes. Hierarchical uncoupling–coupling of metastable conformations. In T. Schlick and H. H. Gan, editors, *Computational Methods for Macromolecules: Challenges and Applications – Proc. of the 3rd Intern. Workshop on Algorithms for Macromolecular Modelling*, pages 235–259, Berlin, Heidelberg, New York, 2002. Springer.

[12] D. Frenkel and B. Smit. *Understanding Molecular Simulation – From Algorithms to Applications*, volume 1 of *Computational Science Series*. Academic Press, 2002.

[13] A. Gelman and D. Rubin. Inference from Iterative Simulation using Multiple Sequences. *Statist. Sci.*, 7:457–511, 1992.

[14] A. Gelman and D. Rubin. Markov chain Monte Carlo Methods in Biostatistics. *Stat. Meth. Med. Res.*, 5:339–355, 1996.

[15] W. Göpel and H.-D. Wiemdörfer. *Statistische Thermodynamik*. Spectrum, Akademischer Verlag, 2000.

[16] C.A. Grob and S. Winstein. Mechanismus der mutarotation von 5,6-dibromcholestan. *Helv. Chim. Acta.*, 35:780–802, 1952.

[17] T.A. Halgren. The representation of van der Waals (vdW) interactions in molecular mechanics force fields: potential form, combination rules, and vdW parameters. *J. Am. Chem. Soc.*, 114:7827–7843, 1992.

[18] T.A. Halgren. Merck molecular force field. *J. Comp. Chem.*, 17(I-V):490–641, 1996.

[19] N.V. Heeb, W.B. Schweizer, M. Kohler, and A.C. Gerecke. Structure elucidation of hexabromocyclododecanes – a class of compounds with a complex stereochemistry. *Chemosphere*, 61:65–73, 2005.

[20] N.V. Heeb, W.B. Schweizer, P. Mattrel, R. Haag, and M. Kohler. Crystal structure analysis of enantiomerically pure (+) and (−) β-hexabromocyclododecanes. *Chemosphere*, 66:1590–1594, 2007.

[21] M. R. Hestens and E. Stiefel. Methods of Conjugate gradients for Solving Linear Systems. *J. Res. Nat. Bur. Stand.*, 49:409–436, 1952.

[22] R. W. Hunziker, S. Gonsior, J. A. MacGregor, D. Desjardins, J. Ariano, and U. Friederich. Fate and Effect of Hexabromocyclododecane in the Environment. *Biol. Photol. Transf.*, 66:2300–2305, 2004.

[23] K. Janak, A. Covaci, S. Voorspoels, and G. Becher. Hexabromocyclododecane in marine species from the western scheldt estuary: Diastereoisomer- and enantiomer-specific accumulation. *Environ. Sci. Technol.*, 39:1987–1994, 2005.

[24] M. Kijima. *Markov Processes for Stochastic Modeling.* Stochastic Modeling Series. Chapman and Hall, 1997.

[25] J.F. King and R. G. Pews. Reaction mechanism studies. 3. solvent effects and nature of transition state in diaxial→diequatorial rearrangement. *Can. J. Chem.*, 43:847–861, 1965.

[26] R. Koeppen and R. Becker. submitted, 2007.

[27] R. Koeppen, R. Becker, F. Emmerling, C. Jung, and I. Nehls. Enantioselective preparative HPLC separation of the HBCD-stereoisomers from the technical product and their absolute structure elucidation using x-ray crystallography. *Chirality*, 19:214–222, 2007.

[28] K. Law, V. P. Palace, T. Halldorson, R. Danell, K. Wautier, B. Evans, M. Alaee, C. Marvin, and G. T. Tomy. Dietary accumulation of hexabromocyclododecane diastereoisomers in juvenile rainbow trout (Oncorhynchus mykiss) I: Bioaccumulation parameters and evidence of bioisomerization. *Environ. Toxicol. Chem.*, 25:1757–1761, 2006.

[29] M. Peled, R. Scharia, and D. Sondack. Thermal rearrangement of hexabromocyclododecane (HBCD). In J. R. Desmurs, B. Gerard, and M.J. Goldstein, editors, *Advances in Organobromine Chemistry*, volume 2, pages 92–99. Elsevier, Amsterdam, Netherlands, 1995.

[30] Ch. Schütte, A. Fischer, W. Huisinga, and P. Deuflhard. A direct approach to conformational dynamics based on hybrid Monte Carlo. *J. Comput. Phys., Special Issue on Computational Biophysics*, 151:146–168, 1999.

[31] Y. Sugita and Y. Okamoto. Replica-exchange molecular dynamics method for protein folding. *Chem. Phys. Letters*, 314:141–151, 1999.

[32] S. Suzuki and A. Hasegawa. Determination of Hexabromocyclododecane Diastereomers and Tetrabromobisphenol A in Water and Sediment by Liquid Chromatography/Mass Spectrometry. *Analytical Sciences*, 22:469–474, 2006.

[33] J.G. Vos, G. Becher, M. van den Berg, M. de Boer, and P.E.G. Leonards. Brominated flame retardants and endocrine disruption. *Pure Appl.Chem.*, 75:2039–2046, 2003.

[34] M. Weber. *Meshless Methods in Conformation Dynamics.* Doctoral thesis, Department of Mathematics and Computer Science, Freie Universität Berlin, 2006. Published by Verlag Dr. Hut, München.

[35] M. Weber. Conformation-Based Transition State Theory. ZIB report 07-18, Zuse Institute Berlin, 2007.

[36] M. Weber, S. Kube, L. Walter, and P. Deuflhard. Stable computation of propability densities for metastable dynamical systems. *SIAM J. Multisc. Mod. Sim.*, 6(2):396–416, 2007.